Alexandria Engineering Journal (2015) 54, 955–971

HOSTED BY

Alexandria University

Alexandria Engineering Journal

www.elsevier.com/locate/aej
www.sciencedirect.com

REVIEW

A Review on the development of lattice Boltzmann computation of macro fluid flows and heat transfer

D. Arumuga Perumal [a,*], Anoop K. Dass [b]

[a] Department of Mechanical Engineering, National Institute of Technology Karnataka, Surathkal, Mangalore 575025, India
[b] Department of Mechanical Engineering, Indian Institute of Technology Guwahati, Guwahati 781039, India

Received 5 October 2013; revised 16 June 2015; accepted 23 July 2015
Available online 26 September 2015

KEYWORDS

Lattice Boltzmann method;
Single-relaxation-time;
Multi-relaxation-time;
Boundary condition;
Lattice kinetic scheme

Abstract The Lattice Boltzmann Method (LBM) is introduced in the Computational Fluid Dynamics (CFD) field as a tool for research and development, but its ultimate importance lies in various industrial and academic applications. Owing to its excellent numerical stability and constitutive versatility it plays an essential role as a simulation tool for understanding micro and macro fluid flows. The LBM received a tremendous impetus with their spectacular use in incompressible and compressible fluid flow and heat transfer problems. The applications of LBM to incompressible flows with simple and complex geometries are much less spectacular. From a computational point of view, the present LBM is hyperbolic and can be solved locally, explicitly, and efficiently on parallel computers. The present paper reviews the philosophy and the formal concepts behind the lattice Boltzmann approach and gives progress in the area of incompressible fluid flows, compressible fluid flows and free surface flows.

Contents

* Corresponding author at: Department of Mechanical Engineering, NIT Karnataka, Surathkal, Karnataka 575025, India. Tel.: +91 91598 60535; fax: +91 361 2690762.
E-mail address: d.perumal@alumni.iitg.ernet.in (D. Arumuga Perumal).
Peer review under responsibility of Faculty of Engineering, Alexandria University.

http://dx.doi.org/10.1016/j.aej.2015.07.015

1. Introduction

1.1. General background

The continuous growth of computer power has motivated the scientific community to use CFD for numerical solution of the governing equations of fluid dynamics [1]. Generally the mathematical models used in CFD include convective and diffusive transport of some variables. These mathematical models consist of governing equations in the form of ordinary or partial differential equations (ODEs or PDEs). As a great number of such model equations like the Navier–Stokes equations do not possess analytical solutions, one has to resort to numerical methods [2]. The difficulty in solving the Navier–Stokes equations is due to their nonlinear terms. In conventional numerical methods, the macroscopic variables of interest such as velocity and pressure are usually obtained by solving the Navier–Stokes equations [3].

Over the years, the finite difference method (FDM) and finite volume method (FVM) are frequently being used in CFD [4]. FDM consists in essentially setting up a uniform rectangular grid in the problem domain, discretizing the governing equations with respect to the grid by replacing the derivatives with their finite-difference approximations and solving the resulting algebraic equations numerically [5]. For non-uniform grids FDM requires a transformation of the physical space onto a computational space with an uniform grid. FVM requires no such transformation as it solves the integral form of the governing equations that are integrated over (generally) irregularly-shaped finite volumes. The finite element method (FEM) has not gained as much popularity in fluid mechanics as it has in structural mechanics.

In the last two decades, a different kind of numerical method for applications in CFD, namely, the Lattice Boltzmann Method (LBM) has gained popularity [6]. The LBM has emerged as a new effective and alternative approach of CFD and it has achieved considerable success in simulating fluid flows and heat transfer problems [7]. In the LBM approach, one solves the kinetic equation for the particle distribution function. The macroscopic variables such as velocity and pressure are obtained by evaluating the hydrodynamic moments of the particle distribution function [8]. One of the most popular and simple approaches in the LBM is lattice Boltzmann equation with linearized collision operator based on the Bhatnagar–Gross–Krook (LBM-SRT) collision model. It is known that, through a Chapman–Enskog analysis, one can recover the governing continuity and momentum equations in the low Mach number limit [9].

1.2. Overview of LBM

In the past few years, researchers have been using lattice Boltzmann method for simulating and modelling in physical, chemical, social systems including flows in magnetohydrodynamics [10], immiscible fluids [11], multiphase flows [12], heat transfer problems [13–15], porous media [16] and isotropic turbulence [17]. Historically, LBM originated from the method of Lattice gas automata (LGA), which was first introduced in 1973 by Hardy, Pomeau and de Pazzis (HPP) [18]. In LGA, the term Lattice implies that one is working on a lattice which is d-dimensional and usually regular. Gas suggests that a gas is moving on the lattice. The gas is usually represented by Boolean particles (0 or 1). Automata indicate that the gas evolves according to a set of rules. In the LGA model, the space, time and particle velocities are all discrete. The iteration of an LGA consists of a collision and propagation step. But, the major drawbacks of the LGA were intrinsic noise, non-Galilean invariance, an unphysical velocity dependent pressure and large numerical viscosities. In 1986, Frisch, Hasslacher and Pomeau (FHP) obtained the correct Navier–Stokes equations using a hexagonal lattice. Lattice Boltzmann equations has been used at the cradle of Lattice Gas Automata (LGA) by Frisch et al. [19] to calculate viscosity. To eliminate statistical noise, in 1988 McNamara and Zanetti [20] did away with the Boolean operation of LGA involving the particle occupation variables by neglecting particle correlations and introducing averaged distribution functions giving rise to the LBM.

Higuera and Jimenez [21] brought about an important simplification in LBM by presenting a Lattice Boltzmann Equation (LBE) with a linearized collision operator that assumes that the distribution is close to the local equilibrium state. A particularly simple version of linearized collision operator based on the Bhatnagar–Gross–Krook (BGK) [22] collision model was independently introduced by several authors including Koelman [23] and Chen et al. [24]. The lattice BGK (LBGK) model [25,26] utilizes the local equilibrium distribution function to recover the macroscopic Navier–Stokes equations.

Boundary condition plays a crucial role in lattice Boltzmann simulations [27–34]. The bounce-back boundary condition is a popular boundary condition in LBM. It is derived from LGA and has been extensively applied in LBM simulations. In this scheme, the particle distribution function

at the wall lattice node is assigned to be the particle distribution function of its opposite direction. The easy implementation of this no-slip velocity condition supports the LBM is ideal for simulating fluid flows. Noble et al. [27] proposed hydrodynamic boundary condition on no-slip walls by enforcing a pressure constraint to replace the bounce-back boundary condition. They simulated steady flow of an incompressible fluid between two infinite parallel plates and demonstrated accurate results by LBM. Inamuro et al. [28] suggested that a slip velocity near wall nodes could be induced by the bounce-back scheme and proposed to use a counter-slip velocity to cancel that effect. Filippova and Hanel [31] proposed curved boundary treatment using Taylor series expansion in both space and time for particle distribution function. In addition, curved boundary treatment was independently introduced by Mei et al. [32] and Bouzidi et al. [33]. A unified scheme for second order accurate curved wall treatment was proposed by Yu et al. [34].

1.3. History of LBM

In the past few decades, the relation between the Boltzmann Equation and Navier–Stokes equation for the study of fluid dynamics has been an active and popular topic of research [35]. The Boltzmann equation relates the time evolution and spatial variation of a collection of molecules to a collision operator that describes the interaction of the molecules. It is known that, the Boltzmann equation provides a more efficient representation of gaseous flows for a whole range of flow regimes than the Navier–Stokes equation. But researchers generally prefer to use the conventional numerical methods (finite difference method, finite volume method, finite element method, etc.) based on the discretization of partial differential equations (Navier–Stokes equations) in continuum regime than solving the Boltzmann equations. This is because solution of the Boltzmann equation is a non-trivial task owing to the complexity of the collision term.

The development of Lattice Gas Automata (LGA) and Lattice Boltzmann Method (LBM) are the promising methods that use different kind of nonconventional techniques for applications in CFD. The LGA, however, suffered from some drawbacks such as lack of Galilean invariance, statistical noise and unphysical solution (pressure depends on velocity). Investigators overcame the difficulties of LGA through the LBM using the simple model of linearized collision operator based on the Bhatnagar–Gross–Krook (LBGK) collision model [9]. The justification for the LBM approach is the fact that the collective behaviour of many microscopic particles is behind the macroscopic dynamics of a fluid and this dynamics is not particularly dependent on the details of the microscopic phenomena exhibited by the individual molecules. It is the solution of a minimal Boltzmann kinetic equation, rather than the discretization of the Navier–Stokes equations of continuum mechanics. It provides stable and efficient numerical calculations for the macroscopic behaviour of fluids, although describing the fluid in a microscopic way.

The lattice model in LBM notation follows a D_xQ_y reference, where x is the number of dimensions and y denotes the number of particle velocities. As an example popular one-dimensional (1-D) model is referred to as the one-dimensional two-velocity (D_1Q_2) model. Other 1-D models are the one-dimensional three-velocity (D_1Q_3) and one-dimensional five-velocity (D_1Q_5) models. Two-dimensional lattice models are two-dimensional seven-velocity (D_2Q_7) and two-dimensional nine-velocity (D_2Q_9) models. The three-dimensional counterparts are the three-dimensional fifteen-velocity (D_3Q_{15}), three-dimensional nineteen-velocity (D_3Q_{19}) and three-dimensional twenty-seven-velocity (D_3Q_{27}) models. In all the above models, the particles move according to a finite, discrete set of velocities.

It is now observed that an increasing number of researchers simply use the LBM as an alternative to conventional numerical methods for the Navier–Stokes equation. As a computational tool, the lattice Boltzmann method differs from incompressible Navier–Stokes equations-based methods as follows [36]:

1. Navier–Stokes equations are second-order partial differential equations (PDEs); the discrete velocity model from which LBM is derived consists of a set of first-order PDEs (kinetic equations).
2. Navier–Stokes equations have nonlinear convection terms; the convection terms in LBM are linear.
3. Lattice Boltzmann Equation (LBE) is a discretized kinetic equation; Navier–Stokes equations can take integral or differential forms.
4. LBM depends on lattice structure; Navier–Stokes equations are in vector form that is independent on the coordinate and grids.
5. The Navier–Stokes solver usually employs iterative procedures to obtain a converged solution; the LBM is explicit in form and do not need iterative procedures.
6. Boundary conditions involving complicated geometries require careful treatments in both Navier–Stokes equations-based and LBM solvers. In LBM, the boundary condition is in the form of particle distribution functions.
7. Due to the kinetic nature of the Boltzmann equation, the physics associated with the molecular level interaction can be incorporated more easily in the LBE model.

Also it is known that there is no continuum assumption involved in the LBM; therefore, its prospect in simulating microflows is quite evident and the choice of using LBM for microflow simulation is a good one owing to the fact that it is based on the Boltzmann equation which is valid for the whole range of the Knudsen number (which is the ratio of the mean free path of molecules to the characteristic length) [37]. The dimensionless Mach number is defined by

$$Ma = \frac{u_0}{c_s} \tag{1}$$

which must fulfil $Ma < 0.3$ to be within incompressible limit. Here, c_s is the speed of sound. The Reynolds number is defined as

$$Re = \frac{u_0 L}{\upsilon} \tag{2}$$

$L = N\delta x$ being the characteristic length, N the number of lattice nodes in the characteristic length, δx the lattice spacing and u_0 the reference velocity of the flow. The lattice spacing δx and lattice timing δt determine the lattice dimensions.

1.4. Boltzmann equation

Historically the lattice Boltzmann method evolved from Lattice Gas Automata (LGA); an alternative interpretation of LBM is

obtained by considering the Boltzmann equation directly. The Boltzmann equation, also known as the Boltzmann transport equation describes the statistical distribution of particles in a fluid. It is an equation for the time evolution of $f(\boldsymbol{r},\boldsymbol{c},t)$, the particle distribution function in the phase space. Phase space can be viewed as a space in which coordinates are given by the position and momentum vectors at the time. The distribution function $f(\boldsymbol{r},\boldsymbol{c},t)$ gives the probability of finding a particular molecule with a given position and momentum. The classic continuum Boltzmann equation is an integro-differential equation for a single particle distribution function $f(\boldsymbol{r},\boldsymbol{c},t)$ and written as [38]

$$\frac{\partial f}{\partial \boldsymbol{t}}+\boldsymbol{c}\cdot\frac{\partial f}{\partial \boldsymbol{r}}+\boldsymbol{F}\cdot\frac{\partial f}{\partial \boldsymbol{c}}=Q(f) \tag{3}$$

where $\boldsymbol{c}$ is the particle velocity, $\boldsymbol{F}$ is the body force and $Q(f)$ is the collision integral. For the two-particle collision one may write

$$Q(f(f_1,f_2))=\int d\boldsymbol{c}_2\int \sigma(\Omega)|c_1-c_2|\left[f'_1f'_2-f_1f_2\right]d\Omega \tag{4}$$

where $\sigma(\Omega)$ is the differential collision cross section for the two particle collision which transforms the velocities from $\{\mathbf{c}_1,\mathbf{c}_2\}$ (incoming) into $\{\boldsymbol{c}'_1,\boldsymbol{c}'_2\}$ (outgoing). One of the major problems when dealing with the Boltzmann equation is the complicated nature of the collision integral $Q(f)$. To facilitate numerical and analytical solutions of the Boltzmann equation, this collision integral is replaced by a simpler expression proposed by He and Luo [9]. This widely used replacement is called the lattice Boltzmann with BGK approximation or single-relaxation-time model and is given by

$$Q_{BGK}(f)=-\frac{f-f^{eq}}{\tau} \tag{5}$$

where τ is a typical single-relaxation-time associated with collision relaxation to the local equilibrium. It may be noted that alternative formulations based on lattice Boltzmann with multi-relaxation-time is also available.

2. LBM methodology

2.1. Lattice Boltzmann Single-Relaxation-Time (LBM-SRT) model

The LBGK model with single-relaxation-time (LBM-SRT), which is a commonly used lattice Boltzmann method, is given by [39]

$$f_i(\mathbf{x}+\boldsymbol{c_i}\Delta t,t+\Delta t)-f_i(\mathbf{x},t)=-\frac{1}{\tau}\left(f_i(\mathbf{x},t)-f_i^{(0)}(\mathbf{x},t)\right) \tag{6}$$

where $f_i(\mathbf{x},t)$ and $f_i^{(0)}(\mathbf{x},t)$ are the particle and equilibrium distribution functions at $(\mathbf{x},t)$, $\boldsymbol{c}_i$ is the particle velocity along the ith direction and τ is the single-relaxation-time parameter that controls the rate of approach to equilibrium. Above Eq. (6) is updated in the following two steps:

$$\text{Collision step}: \quad \tilde{f}_i(\mathbf{x},t)=f_i(\mathbf{x},t)-\frac{1}{\tau}\left[f_i(\mathbf{x},t)-f_i^{eq}(\mathbf{x},t)\right] \tag{7}$$

$$\text{Streaming step}: \quad f_i(\mathbf{x}+\boldsymbol{c_i}\Delta t,t+\Delta t)=\tilde{f}_i(\mathbf{x},t) \tag{8}$$

where f_i and $\tilde{f}_i$ denote the pre- and post-collision states of the distribution function, respectively. For simulating two-dimensional flows, the two-dimensional nine-velocity model ($D2Q9$) with nine discrete velocities $\boldsymbol{c_i}(i=0,1\ldots,8)$ is commonly used. In a $D2Q9$ square lattice each node has eight neighbours connected by eight links as shown in Fig. 1. Particles residing on a node move to their nearest neighbours along these links in unit time step. The occupation of the rest particle is designated as f_0. The occupation of the particles moving along the x- and y-axes is designated as f_1,f_2,f_3 and f_4, while the occupation of diagonally moving particles is designated as f_5,f_6,f_7 and f_8. The macroscopic quantities such as density ρ and momentum density $\rho\boldsymbol{u}$ are obtained as velocity moments of the distribution function f_i as follows:

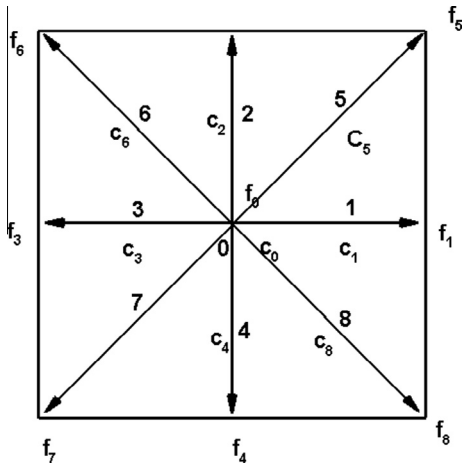

Figure 1 Two-dimensional nine-velocity square lattice model.

$$\rho=\sum_{i=0}^{N}f_i, \tag{9}$$

$$\rho\boldsymbol{u}=\sum_{i=0}^{N}f_i\boldsymbol{c_i} \tag{10}$$

where $N=8$. In LBM, pressure can be directly computed from the equation of state

$$p=\rho c_s^2 \tag{11}$$

where c_s is equal to $1/\sqrt{3}$. The density is determined from the particle distribution function. The density and the velocities satisfy the Navier–Stokes equations in the low-Mach number limit. This can be demonstrated by using the Chapman-Enskog expansion. In the $D2Q9$ square lattice, a suitable equilibrium distribution function that has been proposed is [39]

$$\begin{aligned}
f_i^{(0)}&=\rho w_i\left[1-\frac{3}{2}\boldsymbol{u}^2\right], \quad i=0\\
f_i^{(0)}&=\rho w_i\left[1+3(\boldsymbol{c_i}\cdot\boldsymbol{u})+4.5(\boldsymbol{c_i}\cdot\boldsymbol{u})^2-1.5\,\boldsymbol{u}^2\right], \quad i=1,2,3,4\\
f_i^{(0)}&=\rho w_i\left[1+3(\boldsymbol{c_i}\cdot\boldsymbol{u})+4.5(\boldsymbol{c_i}\cdot\boldsymbol{u})^2-1.5\,\boldsymbol{u}^2\right], \quad i=5,6,7,8
\end{aligned} \tag{12}$$

where the lattice weights are given by $w_0=4/9, w_1=w_2=w_3=w_4=1/9$ and $w_5=w_6=w_7=w_8=1/36$. The relaxation time that fixes the rate of approach to equilibrium is related to the viscosity by [39]

$$\tau=\frac{6\upsilon+1}{2} \tag{13}$$

where υ is the kinematic viscosity measured in lattice units. It is seen that $\tau = 0.5$ is the critical value for ensuring a non-negative kinematic viscosity. Numerical instability can occur for a τ close to this critical value. This situation takes place at high Reynolds numbers. For simulating three-dimensional flows, the fifteen-velocity model $(D3Q15, i = 0, 1, \ldots, 14)$ the nineteen-velocity model $(D3Q19, i = 0, 1, \ldots, 18)$ and the twenty-seven-velocity model $(D3Q27, i = 0, 1, \ldots, 26)$ are used. Fig. 2 shows the *D3Q15, D3Q19 and D3Q27* cubic lattice models. All the above 3D LBM models incorporate a rest particle in the discrete velocity set $\{\boldsymbol{c}_i\}$, because the LBM models with a rest particle have better computational stability and reliability. We now give the discrete particle velocities and weights associated with the commonly used models.

For the $D2Q9$ model the discrete velocity set $\{\boldsymbol{c}_i\}$ is written as [39]

$$\mathbf{c}_i = \begin{cases} 0, & i = 0 \\ c(\cos((i-1)\pi/4), \sin((i-1)\pi/4), & i = 1, 2, 3, 4, \\ \sqrt{2}c(\cos((i-1)\pi/4), \sin((i-1)\pi/4), & i = 5, 6, 7, 8 \end{cases} \tag{14}$$

and the lattice weights are

$$w_i = \begin{cases} 4/9, & i = 0; \\ 1/9, & i = 1, 2, 3, 4; \\ 1/36, & i = 5, 6, 7, 8 \end{cases} \tag{15}$$

For the $D3Q15$ model the discrete velocity set $\{c_i\}$ can be expressed as [40]

$$\boldsymbol{c}_i = \begin{cases} (0, 0, 0), & i = 0; \\ c(\pm 1, 0, 0), c(0, \pm 1, 0), c(0, 0, \pm 1), & i = 1, 2, \ldots, 6; \\ c(\pm 1, \pm 1, \pm 1), & i = 7, 8, \ldots, 14 \end{cases} \tag{16}$$

and the lattice weights are

$$w_i = \begin{cases} 2/9, & i = 0; \\ 1/9, & i = 1, 2, \ldots, 6; \\ 1/72, & i = 7, 8, \ldots, 14 \end{cases} \tag{17}$$

For the $D3Q19$ model the discrete velocity set $\{c_i\}$ can be expressed as [40]

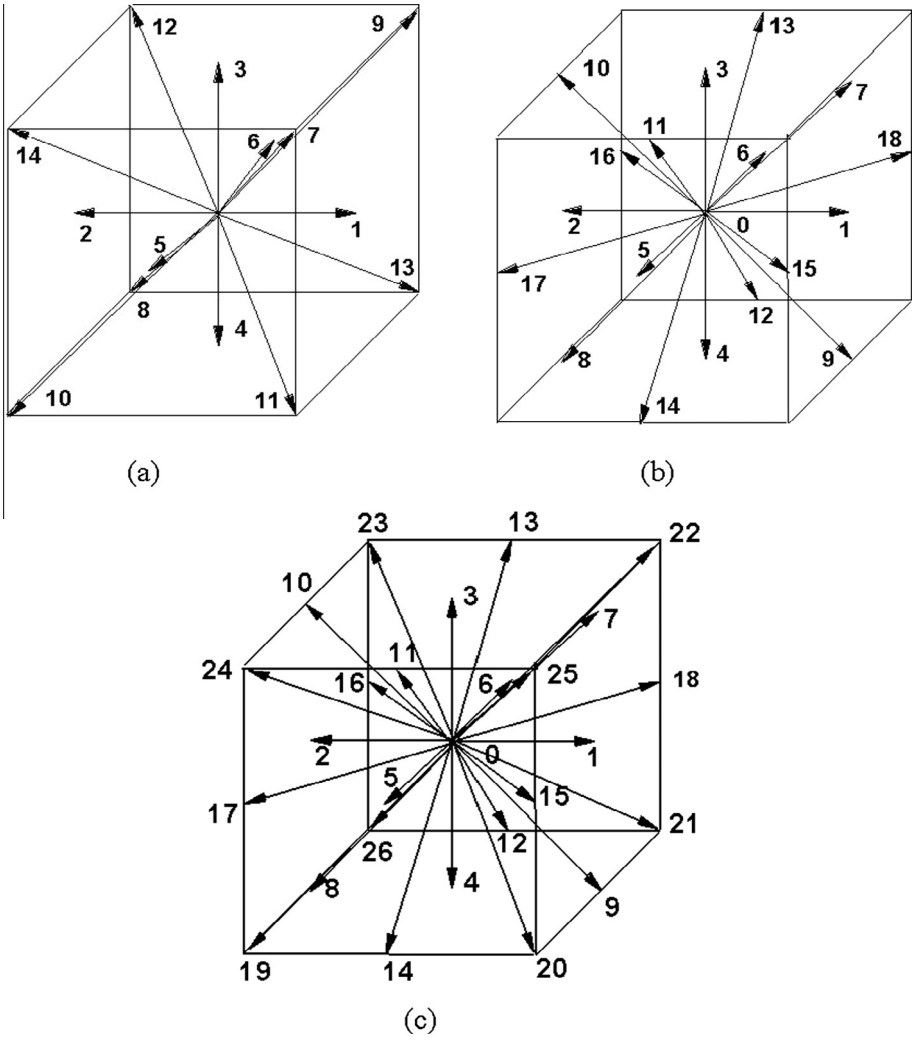

Figure 2 Three-dimensional lattice models: (a) $D3Q15$, (b) $D3Q19$, and (c) $D3Q27$.

$$\boldsymbol{c_i} = \begin{cases} (0,0,0), & i=0; \\ c(\pm1,0,0), c(0,\pm1,0), c(0,0,\pm1), & i=1,2,\ldots,6; \\ c(\pm1,\pm1,0), c(\pm1,0,\pm1), c(0,\pm1,\pm1), & i=7,8,\ldots,18 \end{cases} \tag{18}$$

and the lattice weights are

$$w_i = \begin{cases} 2/9, & i=0; \\ 1/18, & i=1,2,\ldots,6; \\ 1/36, & i=7,8,\ldots,18 \end{cases} \tag{19}$$

For the $D3Q27$ model the discrete velocity set $\{c_i\}$ can be expressed as [40]

$$\boldsymbol{c_i} = \begin{cases} (0,0,0), & i=0; \\ c(\pm1,0,0), c(0,\pm1,0), c(0,0,\pm1), & i=1,2,\ldots,6; \\ c(\pm1,\pm1,0), c(\pm1,0,\pm1), c(0,\pm1,\pm1), & i=7,8,\ldots,18; \\ c(\pm1,\pm1,\pm1), & i=19,20,\ldots,26 \end{cases} \tag{20}$$

and the lattice weights are

$$w_i = \begin{cases} 8/27, & i=0; \\ 2/27, & i=1,2,\ldots,6; \\ 1/54, & i=7,8,\ldots,18; \\ 1/216, & i=19,20,\ldots,26 \end{cases} \tag{21}$$

2.2. Lattice Boltzmann Multi-Relaxation-Time (LBM-MRT) model

Lallemand and Luo [41] showed the robustness of the Lattice Boltzmann Method with multi-relaxation-time (LBM-MRT) model and presented high accuracy results and numerical stability of high Reynolds numbers. They have performed the detailed theoretical analysis on the dispersion, dissipation and stability characteristics of a generalized Lattice Boltzmann Equation model proposed by d'Humieres [42]. For simulating 2D flows a $D2Q9$ model is used and the discrete particle velocities are represented as $\{\boldsymbol{c_i}|i=0,1,\ldots,N\}$ and the particle distribution function is represented as $\{f_i(\mathbf{x},t)|i=0,1,\ldots,N\}$.

The discretized particle distribution function in a vector space R can be written as

$$|f_i(\mathbf{x_i},t_n)\rangle = \{f_0(\mathbf{x_i},t_n), f_1(\mathbf{x_i},t_n),\ldots,f_N(\mathbf{x_i},t_n)\}^T \tag{22}$$

The lattice Boltzmann multi-relaxation-time (LBM-MRT) model evolution equation can be written in discretized form [43]

$$|f_i(\mathbf{x_i}+\boldsymbol{c_i}\Delta t, t_n+\Delta t)\rangle - |f_i(\mathbf{x_i},t_n)\rangle = -M^{-1}\underline{S}(|m_i(\mathbf{x_i},t_n)\rangle - |m_i^{eq}(\mathbf{x_i},t_n)\rangle) \tag{23}$$

where $\underline{S}$ is the diagonal matrix, M for the $D2Q9$ model is a 9×9 transformation matrix that linearly transforms the velocity distribution functions f_i to the macroscopic moments. The transformation matrix M for the $D2Q9$ model can be written as

$$M = \begin{pmatrix} 1 & 1 & 1 & 1 & 1 & 1 & 1 & 1 & 1 \\ -4 & -1 & 2 & -1 & 2 & -1 & 2 & -1 & 2 \\ 4 & -2 & 1 & -2 & 1 & -2 & 1 & -2 & 1 \\ 0 & 1 & 1 & 0 & -1 & -1 & -1 & 0 & 1 \\ 0 & -2 & 1 & 0 & -1 & 2 & -1 & 0 & 1 \\ 0 & 0 & 1 & 1 & 1 & 0 & -1 & -1 & -1 \\ 0 & 0 & 1 & -2 & 1 & 0 & -1 & 2 & -1 \\ 0 & 1 & 0 & -1 & 0 & 1 & 0 & -1 & 0 \\ 0 & 0 & 1 & 0 & -1 & 0 & 1 & 0 & -1 \end{pmatrix} \tag{24}$$

The moments for the $D2Q9$ model are $|m_i\rangle = (\rho, e, \varepsilon, j_x, q_x, j_y, q_y, p_{xx}, p_{xy})^T$. Here ρ is the fluid density, e is the energy, ε is related to square of energy, j_x and j_y are the momentum density (mass flux), q_x and q_y are the energy flux, p_{xx} and p_{xy} correspond to the diagonal and off-diagonal component of the viscous stress tensor. Diagonal matrix ($\underline{S}$) can be written as $\underline{S} = (0, s_2, s_3, 0, s_5, 0, s_7, s_8, s_9)$. The transformation matrix M for the $D3Q15$ model can be written as [41]
The moments for the $D3Q15$ model are

$$|m_i\rangle = (\rho, e, \varepsilon, j_x, q_x, j_y, q_y, j_z, q_z, 3p_{xx}, p_{ww}, p_{xy}, p_{yz}, p_{zx}, t_{xyz})^T.$$

The relaxation rates set as follows $\underline{S} = (0, s_e, s_\varepsilon, 0, s_q, 0, s_q, 0, s_\upsilon, s_\upsilon, s_\upsilon, s_\upsilon, s_\upsilon, s_\upsilon, s_t)$.

$$M = \begin{pmatrix} 1 & 1 & 1 & 1 & 1 & 1 & 1 & 1 & 1 & 1 & 1 & 1 & 1 & 1 & 1 \\ -2 & -1 & -1 & -1 & -1 & -1 & -1 & 1 & 1 & 1 & 1 & 1 & 1 & 1 & 1 \\ 16 & -4 & -4 & -4 & -4 & -4 & -4 & -4 & 1 & 1 & 1 & 1 & 1 & 1 & 1 \\ 0 & 1 & -1 & 0 & 0 & 0 & 0 & 1 & -1 & 1 & -1 & 1 & -1 & 1 & -1 \\ 0 & -4 & 4 & 0 & 0 & 0 & 0 & 1 & -1 & 1 & -1 & 1 & -1 & 1 & -1 \\ 0 & 0 & 0 & 1 & -1 & 0 & 0 & 1 & 1 & -1 & -1 & 1 & 1 & -1 & -1 \\ 0 & 0 & 0 & -4 & 4 & 0 & 0 & 1 & 1 & -1 & -1 & 1 & 1 & -1 & -1 \\ 0 & 0 & 0 & 0 & 0 & 1 & -1 & 1 & 1 & 1 & 1 & -1 & -1 & -1 & -1 \\ 0 & 0 & 0 & 0 & 0 & -4 & 4 & 1 & 1 & 1 & 1 & -1 & -1 & -1 & -1 \\ 0 & 2 & 2 & 0 & -1 & -1 & -1 & -1 & 0 & 0 & 0 & 0 & 0 & 0 & 0 \\ 0 & 0 & 0 & 1 & 1 & -1 & -1 & 0 & 0 & 0 & 0 & 0 & 0 & 0 & 0 \\ 0 & 0 & 0 & 0 & 0 & 0 & 0 & 1 & -1 & -1 & 1 & 1 & -1 & -1 & 1 \\ 0 & 0 & 0 & 0 & 0 & 0 & 0 & 1 & 1 & -1 & -1 & -1 & -1 & 1 & 1 \\ 0 & 0 & 0 & 0 & 0 & 0 & 0 & 1 & -1 & 1 & -1 & -1 & 1 & -1 & 1 \\ 0 & 0 & 0 & 0 & 0 & 0 & 0 & 1 & -1 & -1 & 1 & -1 & 1 & 1 & -1 \end{pmatrix} \tag{25}$$

The transformation matrix M for the $D3Q19$ model can be written as [41]
The moments for the $D3Q19$ model are

$$M=\begin{pmatrix}
1 & 1 & 1 & 1 & 1 & 1 & 1 & 1 & 1 & 1 & 1 & 1 & 1 & 1 & 1 & 1 & 1 & 1 & 1\\
-30 & -11 & -11 & -11 & -11 & -11 & -11 & 8 & 8 & 8 & 8 & 8 & 8 & 8 & 8 & 8 & 8 & 8 & 8\\
12 & -4 & -4 & -4 & -4 & -4 & 4 & 1 & 1 & 1 & 1 & 1 & 1 & 1 & 1 & 1 & 1 & 1 & 1\\
0 & 1 & -1 & 0 & 0 & 0 & 0 & 1 & -1 & 1 & -1 & 1 & -1 & 1 & -1 & 0 & 0 & 0 & 0\\
0 & -4 & 4 & 0 & 0 & 0 & 0 & 1 & -1 & 1 & -1 & 1 & -1 & 1 & -1 & 0 & 0 & 0 & 0\\
0 & 0 & 0 & 1 & -1 & 0 & 0 & 1 & 1 & -1 & -1 & 0 & 0 & 0 & 0 & 1 & -1 & 1 & -1\\
0 & 0 & 0 & -4 & 4 & 0 & 0 & 1 & 1 & -1 & -1 & 0 & 0 & 0 & 0 & 1 & -1 & 1 & -1\\
0 & 0 & 0 & 0 & 0 & 1 & -1 & 0 & 0 & 0 & 0 & 1 & 1 & -1 & -1 & 1 & 1 & -1 & -1\\
0 & 0 & 0 & 0 & 0 & -4 & 4 & 0 & 0 & 0 & 0 & 1 & 1 & -1 & -1 & 1 & 1 & -1 & -1\\
0 & 2 & 2 & -1 & -1 & -1 & -1 & 1 & 1 & 1 & 1 & 1 & 1 & 1 & 1 & -2 & -2 & -2 & -2\\
0 & -4 & -4 & 2 & 2 & 2 & 2 & 1 & 1 & 1 & 1 & 1 & 1 & 1 & 1 & -2 & -2 & -2 & -2\\
0 & 0 & 0 & 1 & 1 & -1 & -1 & 1 & 1 & 1 & 1 & -1 & -1 & -1 & -1 & 0 & 0 & 0 & 0\\
0 & 0 & 0 & -2 & -2 & 2 & 2 & 1 & 1 & 1 & 1 & -1 & -1 & -1 & -1 & 0 & 0 & 0 & 0\\
0 & 0 & 0 & 0 & 0 & 0 & 0 & 1 & -1 & -1 & 1 & 0 & 0 & 0 & 0 & 0 & 0 & 0 & 0\\
0 & 0 & 0 & 0 & 0 & 0 & 0 & 0 & 0 & 0 & 0 & 0 & 0 & 0 & 0 & 1 & -1 & -1 & 1\\
0 & 0 & 0 & 0 & 0 & 0 & 0 & 0 & 0 & 0 & 0 & 1 & 1 & -1 & -1 & 0 & 0 & 0 & 0\\
0 & 0 & 0 & 0 & 0 & 0 & 0 & 1 & -1 & 1 & -1 & -1 & 1 & -1 & 1 & 0 & 0 & 0 & 0\\
0 & 0 & 0 & 0 & 0 & 0 & 0 & -1 & -1 & 1 & 1 & 0 & 0 & 0 & 0 & 1 & -1 & 1 & -1\\
0 & 0 & 0 & 0 & 0 & 0 & 0 & 0 & 0 & 0 & 0 & 1 & 1 & -1 & -1 & -1 & -1 & 1 & 1
\end{pmatrix} \tag{26}$$

$$|m_i\rangle = (\rho, e, \varepsilon, j_x, q_x, j_y, q_y, j_z, q_z, 3p_{xx}, 3\pi_{xx}, p_{ww}, \pi_{ww}, p_{xy}, p_{yz}, p_{zx}, t_x, t_y, t_z)^T.$$

The relaxation rates for the $D3Q19$ model set as follows $\underline{S} = (0, s_e, s_\varepsilon, 0, s_q, 0, s_q, 0, s_q, s_v, s_\pi, s_v, s_\pi, s_v, s_v, s_v, s_t, s_t, s_t)$. The LBM-MRT model introduces much less spatial oscillations near geometrical singular points, which is important for the successful simulation of higher Reynolds number flows. We can conclude that the LBM-MRT model is superior to LBM-SRT model in simulating higher Reynolds number flows having geometrical singularity with much less spatial oscillations due to the different relaxation rates for different physical modes embedded in the MRT scheme.

2.3. Thermal flows

The governing equations for the internal energy density distribution function (IEDDF) model become [44]

$$f_i(\mathbf{x}+\boldsymbol{c_i}\Delta t, t+\Delta t) - f_i(\mathbf{x},t) = -\frac{1}{\tau_v}\left(f_i(\boldsymbol{x},t) - f_i^{eq}(\mathbf{x},t)\right) + F_i \tag{27}$$

$$g_i(\mathbf{x}+\boldsymbol{c_i}\Delta t, t+\Delta t) - g_i(\mathbf{x},t) = -\frac{1}{\tau_c}\left(g_i(\mathbf{x},t) - g_i^{eq}(\mathbf{x},t)\right) \tag{28}$$

where $f_i(\mathbf{x},t)$ is the density distribution function, $f_i^{eq}(\mathbf{x},t)$ is the equilibrium density distribution function, $g_i(\mathbf{x},t)$ is the internal energy distribution function and $g_i^{eq}(\mathbf{x},t)$ is the equilibrium internal energy distribution function at $\mathbf{x}, t$. The equilibrium distribution function for the density $f_i^{eq}(\mathbf{x},t)$ can be written as Eq. (12). For the $D2Q9$ model the equilibrium internal energy distribution function can be written as [44]

$$\begin{aligned}
g_0^{eq} &= -\frac{2\rho e}{3}\frac{\boldsymbol{u}^2}{2c^2}\\
g_{1,2,3,4}^{eq} &= \frac{\rho e}{9}\left[\frac{3}{2} + \frac{3(\boldsymbol{c_i}\cdot\boldsymbol{u})}{2c^2} + \frac{9(\boldsymbol{c_i}\cdot\boldsymbol{u})^2}{2c^4} - \frac{3\,\boldsymbol{u}^2}{2c^2}\right]\\
g_{5,6,7,8}^{eq} &= \frac{\rho e}{36}\left[3 + \frac{6(\boldsymbol{c_i}\cdot\boldsymbol{u})}{c^2} + \frac{9(\boldsymbol{c_i}\cdot\boldsymbol{u})^2}{2c^4} - \frac{3\,\boldsymbol{u}^2}{2c^2}\right]
\end{aligned} \tag{29}$$

For the $D2Q9$ model density relaxation parameter τ_v is related to the kinematic viscosity υ by

$$\upsilon = \left(\tau_v - \frac{1}{2}\right)c_s^2\Delta t \tag{30}$$

and the internal energy relaxation parameter τ_c is related to the thermal diffusivity α by

$$\alpha = \frac{2}{3}\left(\tau_c - \frac{1}{2}\right)\Delta t \tag{31}$$

where c_s is the lattice speed of sound equal to 1/3. Then the macroscopic density, velocity and temperature are calculated by

$$\begin{aligned}
\rho &= \sum_{i=0}^{N} f_i,\\
\rho\boldsymbol{u} &= \sum_{i=0}^{N} f_i\boldsymbol{c_i},\\
\rho e &= \sum_{i=0}^{N} g_i.
\end{aligned} \tag{32}$$

where the internal energy, e, for two-dimensional flows is given by $e = RT$ and for three-dimensional flows is given by $e = 3RT/2$. Here R is the gas constant and temperature of the fluid is described by the internal energy e. The macroscopic density and velocity field are simulated using the density distribution function and the macroscopic temperature is simulated using the internal energy distribution function. Eq. (27) can recover the mass and momentum equations, while Eq. (28) can recover the energy equation at the macroscopic level through the Chapman–Enskog expansion [44].

2.4. Boundary conditions

Boundary Conditions and initial conditions are essential for any CFD methods. In LBM several boundary conditions have been proposed [27–34]. Implementation of boundary conditions in LBM is an important task owing to the fact that one has to translate given information from macroscopic variables to particle distribution function (f_i), since it is the only variable to be evaluated in LBM.

2.4.1. Periodic boundary conditions

Periodic boundary conditions are the simplest instance of boundary conditions. To illustrate the idea, let us take the $D2Q9$ model (Fig. 3) as an example and consider only the direction along the x-axis. After streaming the unknown distribution functions for inlet are f_1, f_5, f_8 and also for outlet are f_3, f_7, f_6.

Inlet (Left boundary)

$$\begin{aligned} f_1(1,y,t) &= f_2(L,y,t) \\ f_5(1,y,t) &= f_5(L,y,t) \\ f_8(1,y,t) &= f_8(L,y,t) \end{aligned} \tag{33}$$

Outlet (Right boundary)

$$\begin{aligned} f_3(L,y,t) &= f_3(1,y,t) \\ f_7(L,y,t) &= f_7(1,y,t) \\ f_6(L,y,t) &= f_6(1,y,t) \end{aligned} \tag{34}$$

2.4.2. Bounce-back boundary conditions

The so-called 'no-slip' boundary condition physically means that there is no flow motion at the boundaries. An implementation of this boundary condition is the so-called bounce-back scheme of the distribution function. The bounce-back boundary condition means that when a particle reaches a wall node, the particle will scatter back to the fluid nodes along its incoming direction. For the $D2Q9$ model (Fig. 3) and considering the bottom wall, after streaming unknown distribution functions f_2, f_5, f_6 are given by

$$\begin{aligned} f_5(x,y,t) &= f_7(x,y,t) \\ f_2(x,y,t) &= f_4(x,y,t) \\ f_6(x,y,t) &= f_8(x,y,t) \end{aligned} \tag{35}$$

This complete reflection guarantees that both tangential and normal components of the wall fluid speed vanish identically.

2.4.2.1. Improved bounce-back boundary condition. To ensure the no-slip boundary condition ($\boldsymbol{U} = 0$) on the wall, Yu et al. [34] suggested a improved bounce-back boundary condition using a linear interpolation formula

$$f_{\bar{i}}(\mathbf{x}_w) = f_i(\mathbf{x}_w) + \frac{\Delta}{1+\Delta}\left(f_i(\mathbf{x}_f + \boldsymbol{c}_i) - f_{\bar{i}}(\mathbf{x}_w)\right) \tag{36}$$

The above boundary condition is valid for both $\Delta < 0.5$ and $\Delta \geqslant 0.5$. For a moving wall they added additional momentum

$$f_{\bar{i}}(\mathbf{x}_w, t+\Delta t) = f_i(\mathbf{x}_w, t+\Delta t) + 2w_i\rho\frac{3}{c^2}\boldsymbol{c}_i \cdot \boldsymbol{u}_w \tag{37}$$

where $f_{\bar{i}}$ indicates post-collision state.

2.4.3. Curved boundary treatment

A curved boundary treatment proposed by Bouzidi et al. [33], which is used on the cylinder surface is written as

$$f_{\bar{i}}(\mathbf{x}_f, t+\Delta t) = \frac{1}{2\Delta}\tilde{f}_{\bar{i}}(\mathbf{x}_f, t) + \frac{2\Delta - 1}{2\Delta}\tilde{f}_{\bar{i}}(\mathbf{x}_f, t) \quad \text{for } \Delta > 1/2 \tag{38}$$

where $f_{\bar{i}}(\mathbf{x}_f, t+\Delta t)$ equivalent to $\tilde{f}_{\bar{i}}(\mathbf{x}, t)$. This boundary condition satisfies the no-slip condition to the second-order in Δx and preserves the geometrical integrity of the wall boundary.

2.4.4. Temperature boundary conditions

For the temperature distribution function, adiabatic walls are simulated by putting the temperature at the sites of the walls equal to the temperature at the nearest sites inside the flow domain. In this thesis, second-order finite difference approximation is used for temperature. As an example, for the top wall in a square cavity $D2Q9$ model [44]

$$g_{i,NY} = \frac{4}{3}g_{i,NY-1} - \frac{1}{3}g_{i,NY-2} \tag{39}$$

where $g_{i,NY}$ is the temperature on the wall; $g_{i,NY-1}$ and $g_{i,NY-2}$ are the temperatures inside the flow domain near the wall.

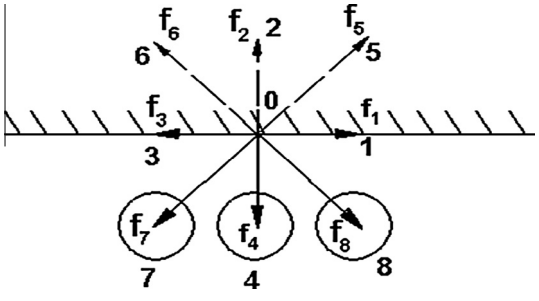

Figure 3 Solid–fluid surface interaction at the top wall.

3. Simulation of macro and micro fluid flows and heat transfer

3.1. Incompressible flows with simple and complex boundaries

The fluid motion inside a closed, square container with rigid walls induced by the tangential motion of a lid constitutes a classical paradigm for internal vortex flows [45–53]. In fact, as hundreds of papers attest, the lid-driven cavity problem is one of the standards used to test new computational schemes. Miller [45] presented two-dimensional lid-driven cavity flow LBM results with Dirichlet and Neumann boundary conditions and results were compared with analytical solutions. Hou et al. [46] extensively studied viscous flow in a square

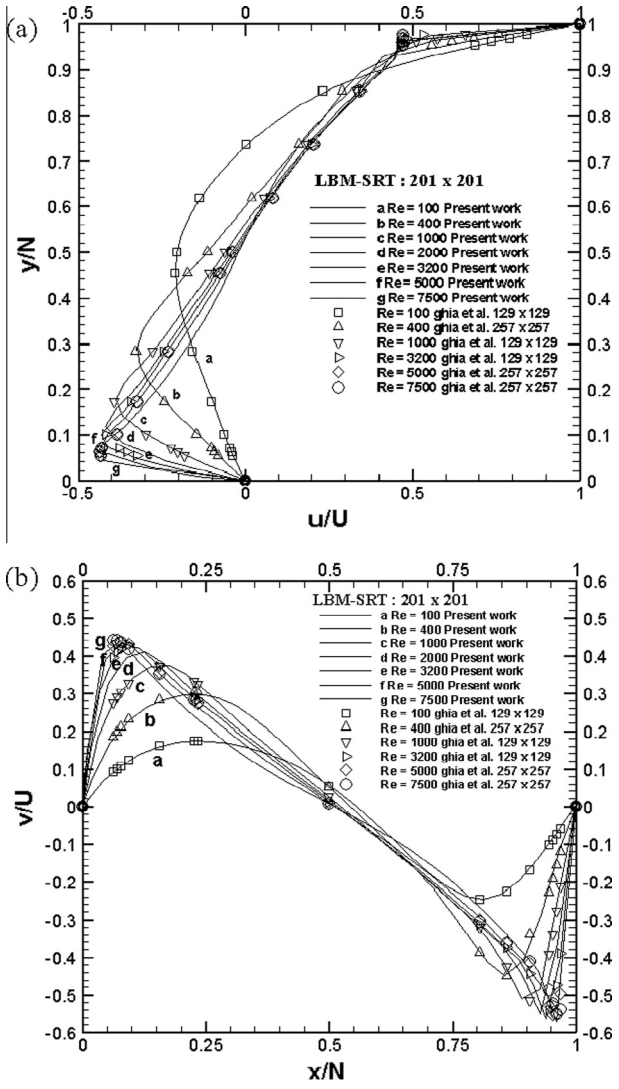

Figure 4 Comparison of LBM-SRT square cavity results: (a) *u*-velocity along the vertical centreline and (b) *v*-velocity along the horizontal centreline.

cavity for a wide range of Reynolds number using LBM-SRT model with bounce-back boundary condition. Some of the notable works in cavity flow by the LBM include those of Shi et al. [47], De et al. [48], Patil and Lakshmisha [49], Shu et al. [50] and Perumal and Dass [51]. There appears to be very little work done on deep cavities by LBM, although they are of more theoretical interest [52,53]. In the lid-driven cavity flow, for a certain Reynolds number by LBM, lid velocity U may be changed within the incompressible Mach number limit. In Fig. 4, we present the horizontal velocities on the vertical centreline and the vertical velocities on the horizontal centreline of the square cavity for Reynolds numbers ranging from 100 to 7500 and compare our data with those of Ghia et al. [54]. In each case, our velocity profiles exhibit a close match with those given by Ghia et al. [54].

To clearly demonstrate and test the advantages of LBM using MRT model over that using SRT model, we compute a lid-driven cavity flow by LBM using both MRT and SRT models. Table 1 shows the strength and location of the primary (1st), secondary (2nd), and ternary (3rd) vortices of the lid-driven square cavity flow. However LBM-MRT method is seen to remove the difficulties faces by the LBM-SRT method at higher Reynolds numbers. Perumal and Dass [55] extended the LBM simulation of two-sided lid-driven square cavity for the parallel and antiparallel wall motion. In the case of parallel motion, besides two primary vortices, there also appears a pair of counter-rotating secondary vortices symmetrically placed about the centreline parallel to the motion of the walls. In the case of antiparallel motion, besides a single primary vortex, there appears two secondary vortices near the trailing edges of the moving walls. The uniqueness of steady flows is almost an article of faith for a given geometry and boundary conditions. But some nonlinear systems in fluid mechanics display multiple-steady solutions for the same set of governing equations and boundary conditions. More recently, the multiplicity of flow states induced by the motion of two-sided non-facing lid-driven square cavity flow and four-sided lid-driven cavity flow using LBM has been investigated by Perumal and Dass [56].

The problem of buoyancy driven square cavity with adiabatic top and bottom walls and differentially heated vertical walls has been the topic of extensive study in the past few

Table 1 The strength and location of the primary (1st), secondary (2nd), and ternary (3rd) vortices of the lid-driven square cavity flow.

Re	Method	(x_{1st}, y_{1st})	(x_{2st}, y_{2st})	(x_{3st}, y_{3st})
1	LBM-SRT Model	(0.4994, 0.7546)	(0.9508, 0.0362)	(0.0343, 0.0364)
	LBM-MRT Model	(0.4994, 0.7528)	(0.9502, 0.0354)	(0.0339, 0.0358)
100	Ghia et al. [54]	(0.6172, 0.7344)	(0.9453, 0.0625)	(0.0313, 0.0391)
	LBM-SRT Model	(0.6152, 0.7361)	(0.9432, 0.0648)	(0.0321, 0.0365)
	LBM-MRT Model	(0.6156, 07366)	(0.9405, 0.0681)	(0.0320, 0.0371)
400	Ghia et al. [54]	(0.5547, 0.6055)	(0.8906, 0.1250)	(0.0508, 0.0469)
	LBM-SRT Model	(0.5537, 0.6041)	(0.8899, 0.1259)	(0.0503, 0.0502)
	LBM-MRT Model	(0.5534, 0.6039)	(0.8896, 0.1247)	(0.0501, 0.0500)
1000	Ghia et al. [54]	(0.5313, 0.5625)	(0.8594, 0.1094)	(0.0859, 0.0781)
	LBM-SRT Model	(0.5304, 0.5616)	(0.8616, 0.1114)	(0.0830, 0.0777)
	LBM-MRT Model	(0.5302, 0.5635)	(0. 8612, 0.1112)	(0.0826, 0.0776)

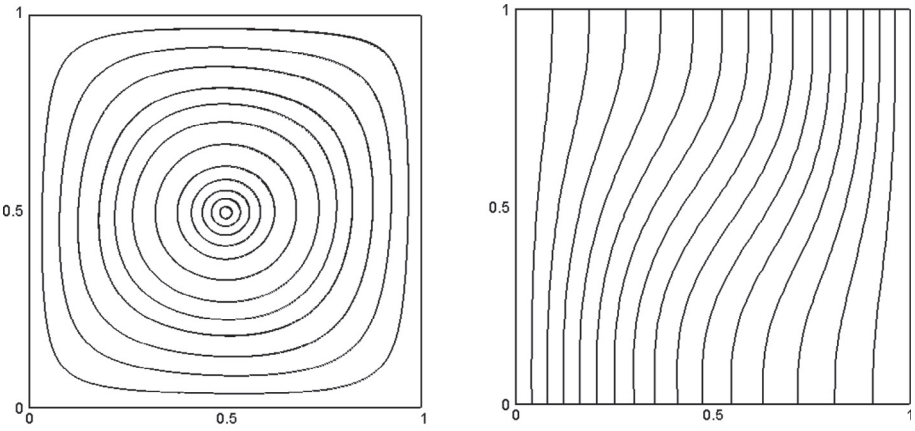

(a) $Ra = 10^3$

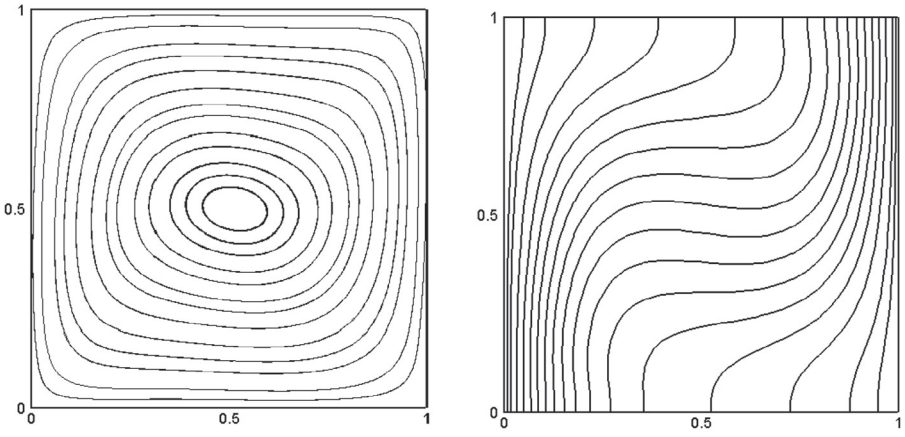

(b) $Ra = 10^4$

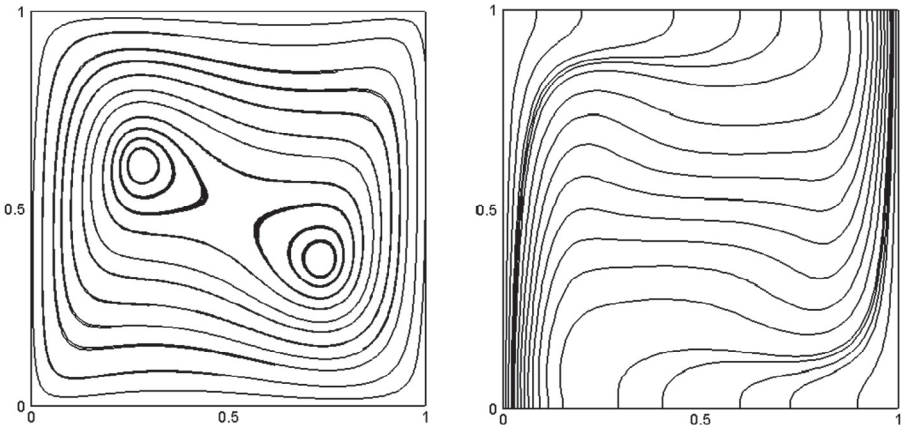

(c) $Ra = 10^5$

Figure 5 streamlines and isotherms for square cavity flow at different Rayleigh number.

decades [57–65]. McNamara et al. [57] were among the first to investigate two-dimensional enclosures using LBM isothermal models. They used only density distribution function in terms of multi-speed approach. Eggels and Somers [58] proposed passive-scalar LBM approach, in which the temperature is simulated using a separate distribution function which is independent of the density distribution function. He et al. [59] developed internal energy density distribution function (IEDDF) approach and it shows greater stability. This model is numerically more stable, and it can incorporate viscous heat dissipation and compression work done by the pressure. Some of the notable works by the LBM include those of Shan [60], Peng et al. [61], Onishi et al. [62], Kuznik et al. [63], Dixit and Babu [64] and Perumal and Dass [65]. Natural convection

problem can be characterized by two dimensionless parameters namely the Rayleigh number Ra and the Prandtl number Pr

$$Ra = \frac{g\beta\Delta TL^3}{\upsilon\alpha}$$
$$Pr = \frac{\upsilon}{\alpha} \tag{40}$$

with g the acceleration due to gravity, β the coefficient of thermal expansion, ΔT the temperature difference between the two vertical walls and L the side of the cavity. Fig. 5 shows the streamlines, isotherms results of the square cavity computations for a fluid of $Pr = 0.71$ with Ra ranging from a moderate to a high laminar regime ($Ra = 10^3$–10^5) are presented through graphs. The lattice Boltzmann method is a relatively novel technique of flow computation, and there is some scope for speculation as to the accuracy of the present LBM computations. Therefore the existing LBM results always has been compared favourably with finite difference methods [66], finite volume methods [67], finite element methods [68], spectral methods [69] and artificial compressibility methods [70].

The LBM is very useful for simulating flows in complicated geometries, such as flow over a cylinder, where wall boundaries are extremely complicated [71–75]. This type of flow problems frequently arises in various engineering fields which offer tough challenges particularly at high Reynolds numbers. In LBM simulation, we use the momentum exchange method to compute the fluid force on the cylinder. The total force acting on a solid body by fluid can be written as [71]

$$F = \sum_{allx_b}\sum_{\alpha=1}^{N_d} e_{\bar{\alpha}}\left[\tilde{f}_\alpha(x_b,t) + \tilde{f}_{\bar{\alpha}}(x_b + e_{\bar{\alpha}}\delta t, t)\right] \times [1 - w(x_b + e_{\bar{\alpha}})]\delta x/\delta t \tag{41}$$

where N_d is the number of nonzero lattice velocity vectors and $w(x_b + e_{\bar{\alpha}})$ is an indicator, which is 0 at x_f and 1 at x_b. The inner summation calculates the momentum exchange between a solid node at x_b, and all possible neighbouring fluid nodes around that solid node. The outer summation calculates the force contributed by all boundary nodes x_b. The two most important characteristic quantities of flow around a cylinder are the coefficient of drag and coefficient of lift. The coefficients are defined as [72]

$$\text{Coefficient of drag } C_D = \frac{F_x}{1/2 \times \rho U_\alpha^2 D}$$
$$\text{Coefficient of lift } C_L = \frac{F_y}{1/2 \times \rho U_\alpha^2 D} \tag{42}$$

where F_x and F_y are the x and y components of the total fluid force acting on the cylinder. U_α is the velocity of the uniform flow and D is the diameter of the cylinder.

The LBM not only computes various steady flows, it has the ability of the present LBM to capture unsteadiness we give the instantaneous streamline and vorticity contour of the circular cylinder time-periodic flow for $Re = 60$ in Fig. 6. Fig. 7 depicts the streamline patterns and vorticity contours for flow past an elliptical cylinder at Reynolds number 100. It is worth mentioning that the numerical simulations of our LBM are much closer to existing available results.

Tolke et al. [76] introduced nonlinear multigrid solution approach for the discrete Boltzmann equation. Mavriplis [77] presented efficient solution strategies for the steady state lattice Boltzmann equation. He checked the ability of the multigrid LBM for the driven cavity. Multigrid techniques applied to LBM are promising but, as occurred in traditional CFD techniques, problems in the prolongation and restriction steps near complex walls have not yet been fully addressed. To increase the numerical accuracy in LBM non-uniform grid has been introduced. He et al. [78] described lattice Boltzmann method to simulate the Navier–Stokes equation on arbitrary non-uniform grids. They presented results of flow in a two-dimensional symmetric channel with sudden expansion. Kuznik et al. [79] simulated natural convection in a square

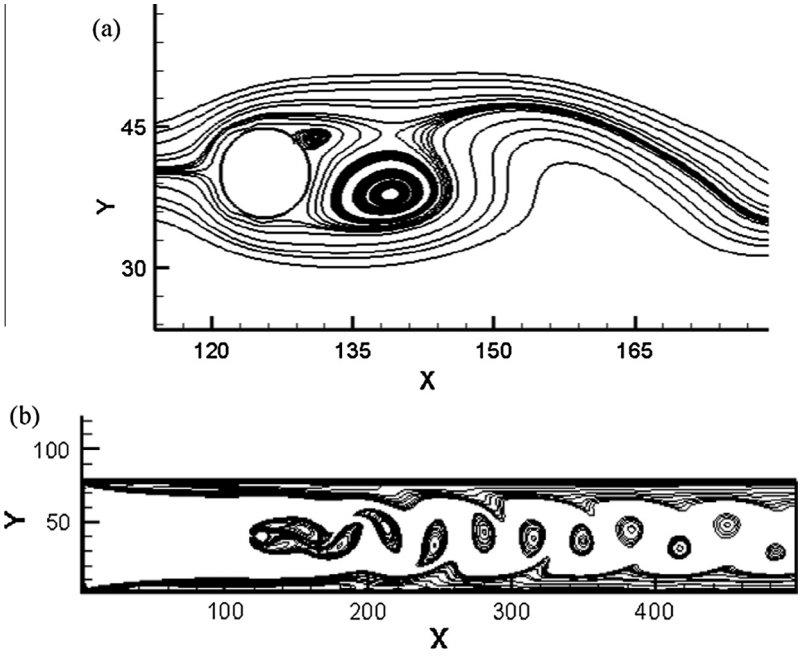

Figure 6 (a) Streamline pattern and (b) vorticity contours for $Re = 60$ for the flow over a circular cylinder. Lattice size: 500 × 80.

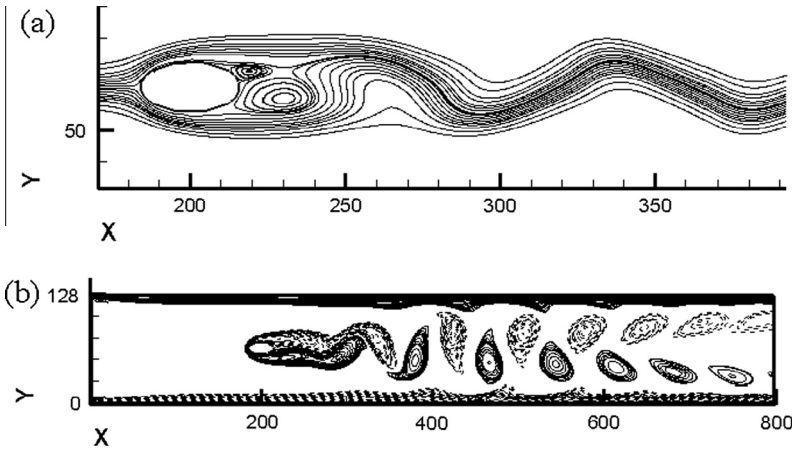

Figure 7 (a) Streamline pattern and (b) vorticity contours for $Re = 100$ for the flow over a elliptic cylinder. Lattice size: 500×80.

cavity using double population lattice Boltzmann method with non-uniform mesh. To maintain the inherent advantage of the LBM, such as simplicity in coding and computational efficiency one prefers to employ the uniform lattice.

As expected, for better flow resolution higher numbers of lattice sizes are required. As the number of lattice size increases the number of time steps to reach the steady state also increases. The finer lattice sizes require more time steps and hence more computing time to reach the steady state. It is known that, non-uniform grids are the lattice points which are un-equally placed. The interpolation formula for non-uniform lattices can be written as [80]

$$f(x) = f(x_0)\frac{(x-x_1)(x-x_2)}{(x_0-x_1)(x_0-x_2)} + f(x_1)\frac{(x-x_0)(x-x_2)}{(x_1-x_0)(x_1-x_2)} + f(x_2)\frac{(x-x_0)(x-x_1)}{(x_0-x_2)(x_2-x_1)} \tag{43}$$

In all the cases, the non-uniform LBM lattices were found to provide accurate results.

A lattice kinetic scheme (LKS) on the 2-D uniform lattice arrangement was proposed by Inamuro [81], based on the standard LBM. In this scheme, we can implement the same standard LBM boundary conditions and it can save computer memory [82]. The derivative term is dropped out and the difficulty of the relatively large viscosity is eased by controlling the time step Δt or speed of sound Cs. If the dimensionless relaxation time τ in Eq. (6) is set to unity, we obtain

$$f_i(\mathbf{x} + \boldsymbol{c_i}\Delta t, t + \Delta t) = f_i^{eq}(\mathbf{x}, t) \tag{44}$$

The relaxation time τ is related to the kinematic viscosity υ by

$$\upsilon = \frac{1}{6}\Delta t \tag{45}$$

The equilibrium distribution functions $f_i^{eq}(\mathbf{x}, t)$ can be expressed in the form as

$$f_i^{(eq)} = \rho w_i\left[1 + 3c_{i\gamma}\boldsymbol{u}_\gamma + \frac{9}{2}c_{i\gamma}c_{i\delta}\boldsymbol{u}_\gamma\boldsymbol{u}_\delta - \frac{9}{2}\boldsymbol{u}_\gamma\boldsymbol{u}_\gamma + A\Delta x\left(\frac{\partial \boldsymbol{u}_\delta}{\partial x_\gamma} + \frac{\partial \boldsymbol{u}_\gamma}{\partial x_\delta}\right)c_{i\gamma}c_{i\delta}\right] \tag{46}$$

where $\gamma, \delta = x, y$ represent Cartesian coordinates (the summation convention is used), and A is a constant parameter of $O(1)$, which determines the fluid viscosity as described below. The parameter A may be regarded as a relaxation parameter of the stress tensor in the generalized lattice Boltzmann equation. Peng et al. [83] extended the LKS for the incompressible viscous thermal flows on arbitrary meshes. More recently, Mendoza et al. [84] presented the LKS to simulate fluid flow problems in curvilinear geometries and curved spaces.

3.2. LBM for compressible euler equations

Numerical solutions of the Euler equations are a highly emerging field in the area CFD. As an alternative CFD tool, the conventional LBM developed in the past suffered from the constraint of small Mach number limit because the particle velocities belong to a discrete set. It is noticed that, two issues should be addressed within the LBM before simulation of Euler compressible flows is pursued. The first one is to increase the allowable Mach number range, and the next one is to incorporate the effects of temperature change into LBM formulations. The LBM for the compressible Navier–Stokes equations was first proposed by Alexander et al. [85]. They presented a selectable sound speed model to simulate compressible flow by the parameters of the equilibrium distribution function appropriately to set the sound speed as low as possible. Chen et al. [86] developed a lattice Boltzmann model without nonlinear deviation terms. Yan et al. [87] presented a two-dimensional nine-bit model with two rest energy levels, which can recover the Euler equation with the streaming and collision process. The Sod and Lax shock tube problem was successfully simulated by this model. Yu and Zhao [88] introduced an attractive force to reduce the sound speed and alleviate the small Mach number restriction. They simulated compressible fluid flows with high Mach numbers up to 5. Palmer and Rector [89] formulated a thermal model that can be used to simulate temperature variations in a compressible flow problem. The compressible Navier–Stokes equations can be written as

$$\begin{aligned}
&\frac{\partial \rho}{\partial t} + \frac{\partial \rho u_\alpha}{\partial x_\alpha} = 0,\\
&\frac{\partial \rho u_\alpha}{\partial t} + \frac{\partial \rho u_\alpha u_\beta}{\partial x_\beta} + \frac{\partial p}{\partial x_\alpha} = \frac{\partial P'_{\alpha\beta}}{\partial x_\beta}\\
&\frac{\partial \rho\left(\frac{1}{2}u_\alpha^2 + bRT\right)}{\partial t} + \frac{\partial \rho\left(\frac{1}{2}u_\alpha^2 + bRT\right)u_\alpha + pu_\alpha}{\partial x_\alpha}\\
&\quad = \frac{\partial}{\partial x_\beta}\left(k\frac{\partial T}{\partial x_\beta} - P'_{\alpha\beta}u_\alpha\right)
\end{aligned} \tag{47}$$

where

$$p = \rho RT,$$
$$P'_{\alpha\beta} = \mu\left(\frac{\partial u_\alpha}{\partial x_\beta} + \frac{\partial u_\beta}{\partial x_\alpha} - \frac{2}{3}\frac{\partial u_\chi}{\partial x_\chi}\delta_{\alpha\beta}\right) + \mu_B \frac{\partial u_\chi}{\partial x_\chi}\delta_{\alpha\beta} \tag{48}$$

Here μ is the viscosity, μ_B is the bulk viscosity and k is the thermal conductivity.

In compressible flow, the equilibrium density distribution function is expressed as

$$f_i^{eq} = \rho w_i(1 + \boldsymbol{c_i}\cdot\boldsymbol{u} + \frac{1}{2}\left((\boldsymbol{c_i}\cdot\boldsymbol{u})^2 - \boldsymbol{u}\cdot\boldsymbol{u} + (\theta-1)(\boldsymbol{c_i}\cdot\boldsymbol{c_i} - D)\right) + \frac{\boldsymbol{c_i}\cdot\boldsymbol{u}}{6}\left((\boldsymbol{c_i}\cdot\boldsymbol{u})^2 - 3(\boldsymbol{u}\cdot\boldsymbol{u}) + 3(\theta-1)(\boldsymbol{c_i}\cdot\boldsymbol{c_i} - D - 2)\right)) \tag{49}$$

where θ is the dimensionless temperature, and D is spatial dimension. The macroscopic density, temperature and velocity are calculated from

$$\rho = \sum_{i=0}^{N} f_i,$$
$$\rho\boldsymbol{u} = \sum_{i=0}^{N} f_i\boldsymbol{c_i} \tag{50}$$
$$\rho(D\theta + \boldsymbol{u}.\boldsymbol{u}) = \sum_{i=0}^{N} f_i\boldsymbol{c_i}.\boldsymbol{c_i}$$

Kataoka and Tsutahara [90] presented a lattice Boltzmann model for the compressible Navier–Stokes equations with a flexible specific-heat ratio. Sun [91] incorporated a large particle-velocity set in a locally adaptive LBM model. Sun and Hsu [92] extended the simulation of adaptive models based on hexagonal lattices to multi level square lattices. They successfully simulated two-dimensional shock-wave propagations and boundary layer flows. He et al. [93] presented the compressible LBM model and they successfully applied to 2D and 3D benchmark compressible flow problems. Li and Zhong [94] proposed the double distribution function model and the governing equations are discretized using the third order monotone upwind scheme for scalar conservation laws finite volume scheme. They recovered compressible continuity, momentum using density distribution function and energy equation is recovered energy distribution function. They also found that the LBM model is suitable for compressible flows, even for strong shock wave problem, which has an extremely large pressure ratio, 100,000.

3.3. LBM simulation of free surface flows

Free surface flow phenomena are ubiquitous in nature and in many industrial applications. To solve free-surface-flow problem, various methods, such as the finite difference method, the finite volume method, the smoothed particle hydrodynamics method and the Lattice Boltzmann Method (LBM), have been proposed. In the last two decades, several approaches have been developed to apply LBM to free-surface problems. Several single-phase free-surface models have been proposed by many authors. For free-surface-flow problems, the ability of a numerical model to handle high viscosity ratios and high density ratios is crucial. Ginzburg and Steiner [95] presented a free-surface LBM model that makes use of more complicated boundary conditions, and prescribes shear stresses at the interface. From a numerical point of view, a free-surface represents a moving boundary, hence, leading to a transient computational domain. To calculate the movement of phase interfaces, an additional advection equation has to be solved in the LBM. In LBM simulation of free surface flows, the computational algorithm can be split into two independent parts: (i) the fluid flow field is calculated with the LBM; (ii) the interface location is updated using a different and independent solver.

Needless to say, for the free-surface LBM model, popular volume of fluid (VOF) approach is used to capture moving interface. For the simulation of free surface flow in a VOF framework, an additional transport equation must be solved for the interface evolution between the two phases. For the solution of the flow field, the LBM is used, where the free surface is represented by a VOF approach. In VOF approach a fluid fraction variable ε is introduced to describe the cell level of a control volume V_{CV}

$$\varepsilon = \frac{V_{fluid}}{V_{CV}} \tag{51}$$

The unknown distribution functions from gas cells are reconstructed through a free-surface boundary condition. Körner et al. [96] combined LBM with a VOF approach and a flux-based advection scheme. Their model was developed for the simulation of metal foams and it is also capable of handling free-surface-flow simulations. The flux terms are expressed directly in terms of LBM distribution functions.

On the other hand, as an alternative choice of VOF method to capture moving interface, the level set method (LSM) was proposed. The movement of the interface is accomplished through the evolution of a distance function ϕ. Compared with volume of fluid methods, level set methods are more accurate. Yu et al. [97] coupled the lattice Boltzmann and particle level set method to simulate free-surface flows. In the level set method distance function can be written as

$$\phi(X) = \begin{cases} 0, & \forall X \in \Gamma \\ -d(X), & \forall X \in \Omega \\ d(X), & \forall X \notin \Omega \end{cases} \tag{52}$$

where $d(X) = \min(|X - X'|)$ for all $X' \in \Gamma$ and Γ represents the interface and Ω refers to the space inside Γ.

Janssen and Krafczyk [98] presented a conservative, finite-volume-based advection scheme for free-surface-flow simulations with LBM, which is inherently suitable for the application on non-uniform, block-structured grids. Wardle and Lee [99] demonstrated the application of a finite element Lattice Boltzmann Equation (FE-LBE) method to the annular mixing geometry as found in a centrifugal contactor. Leonardi et al. [100] developed a coupled discrete element method (DEM)-LBM model for the free-surface simulation of heterogeneous suspensions. They employed the LBM for non-Newtonian rheology, free-surfaces and moving boundaries.

3.4. Fluid Flows in MEMS

In the past few years there has been significant progress in the development of Micro-electro-mechanical systems (MEMS) at the application and as well as at the simulation levels [101]. It is known that, the laws of fluid motion for microfluidic systems

are different from those that of large scale (macro) systems in terms of forces and surface effects. Traditional numerical simulations rely on continuum approach and the Navier–Stokes equations break down at higher values of the Knudsen number Kn which equals the ratio of the mean free path of the gas molecules λ to the characteristic length L of the flow system [102]. In the micro-scale geometries Kn is generally high and the Navier–Stokes equation loses validity. It is accepted that the Navier–Stokes equations with no-slip boundary conditions are only appropriate when $Kn < 0.001$. The gas flow for $0.001 < Kn < 0.1$ is termed slip regime and $0.1 < Kn < 10$ is termed transition regime. For $Kn > 10$ the system can be considered as a free molecular flow regime. Raabe [103] discussed extensively about LBM for micro- and nano-scale fluid dynamics in the area of materials science and engineering.

The Lattice Boltzmann Equation (LBE) which can be linked to the Boltzmann equation in kinetic theory is formulated as [104]

$$f_i(\mathbf{x} + c_i\Delta t, t + \Delta t) - f_i(\mathbf{x}, t) = -\frac{1}{\tau}\left(f_i(\mathbf{x}, t) - f_i^{(0)}(\mathbf{x}, t)\right) \tag{53}$$

Here, f_i is the set of discrete populations representing the probability of finding a particle at position $\mathbf{x}$ at time t moving along the direction identified by the discrete particle velocity c_i, i is the number of links at each point and τ is the time relaxation parameter. To simulate microscopic gaseous flows LBM relates the relaxation time τ to the Knudsen number from the kinetic theory. Lim et al. [105] related τ to Knudsen number Kn

$$\tau = Kn(N_y - 1) \tag{54}$$

where N_y is the number of lattice nodes in y-direction.

Nie et al. [106] explored the possibility of using LBM-SRT model to simulate fluid flows with high Knudsen number. They concluded that the LBM-SRT model is a Boltzmann equation in kinetic theory based on the particle distribution functions, and it can be used to study the flow dependence on Knudsen number, including the slip velocity, the nonlinear pressure drop in micro-channel, and the variation in the vortex centre in the micro-cavity. Three slip boundary conditions, namely diffuse scattering boundary condition (DSBC), specular reflection and a combination of bounce-back and specular reflection boundary condition are commonly used to predict the flow fields. The specular reflection means the particle will reflect in the specular direction like a ray of light. DSBC is derived from the gas surface interaction law of the kinetic theory. The DSBC of the LBM is as follows

$$|(\boldsymbol{e}_i - \boldsymbol{u}_w)\cdot\boldsymbol{n}|f_i = \sum_{(\boldsymbol{e}_{i'} - \boldsymbol{u}_w)\cdot\boldsymbol{n}<0} |(\boldsymbol{e}_{i'} - \boldsymbol{u}_w)\cdot\boldsymbol{n}|\Re_f(\boldsymbol{e}_{i'} \to \boldsymbol{e}_i)f_{i'} \tag{55}$$

where $\boldsymbol{e}_i$ and $\boldsymbol{e}_i'$ are the molecular velocities of the incident and reflected particles, respectively, $\boldsymbol{n}$ is the inward unit normal vector of the wall and w indicates the wall boundary. Ansumali et al. [107] presented results using Entropic Lattice Boltzmann Method (ELBM) for low Mach and low Knudsen number hydrodynamics pertinent to microflows and reported that their results can complement or even replace computationally expensive microscopic simulation techniques such as kinetic Monte Carlo method and/or molecular dynamics. Verhaeghe et al. [108] implement the athermal LBM-MRT with a first-order slip velocity model and demonstrate that the LBE method can be used to simulate gaseous flow through a long micro-channel in the slip flow regime. Alapati et al. [109] presented the simulation of two-phase flow in a three-dimensional cross-junction microchannel by LBM. Suga [110] has provided a study on LBM for complex micro-flows in the slip and transitional regime. It is concluded that the applicability of the micro-flow LBM for complex flow predicts very well.

4. Conclusions

Selected literature on lattice Boltzmann computation of macro fluid flows and heat transfer over a period of two decades has been presented in this paper. The lattice Boltzmann method has made a substantial progress since the early nineteen nineties till today, especially in the computation of incompressible viscous flow and heat transfer problems. The LBM simulation for compressible and free surface flows has been an interesting and active topic of research in recent days. Since its inception many attempts have been made to apply the method to attack many complex fluid-flow and heat transfer problems that were earlier the traditional bastions of the continuum-based methods such as the finite difference, finite volume and finite element so as to establish it as a credible alternative to these methods. Therefore, LBM is used to solve a variety of fluid-flow and heat-transfer problems in the micro and macro regimes of flow, thus demonstrating that it has already established itself as an important alternative solution procedure in CFD. As already reported, LBM has made deep inroads into the computation of micro and macro fluid flows with simple and complex geometries. The potential of LBM still remains to explore many more areas and breaks new grounds.

References

[1] T.J. Chung, Computational Fluid Dynamics, Cambridge University Press, Cambridge, 2002.
[2] Y. Sone, Kinetic Theory and Fluid Dynamics, Birkhauser, Boston, 2002.
[3] S. Succi, The Lattice Boltzmann Method for Fluid Dynamics and Beyond, Oxford University Press, 2001.
[4] D.A. Perumal, A.K. Dass, Simulation of incompressible flows in two-sided lid-driven square cavities. Part I – FDM, CFD Lett. 2 (2010) 13–24.
[5] D.A. Perumal, Simulation of flow in Two-Sided Lid-Driven deep cavities by finite difference method, J. Appl. Sci. Thermodyn. Fluid Mech. 6 (2012) 1–6.
[6] J.M. Yeomans, Mesoscale simulations lattice Boltzmann and particle algorithms, Phys. A 369 (2006) 159–184.
[7] S. Chen, G.D. Doolen, Lattice Boltzmann method for fluid flows, Annu. Rev. Fluid Mech. 30 (1998) 282–300.
[8] X. He, L.S. Luo, A priori derivation of the lattice Boltzmann equation, Phys. Rev. E 55 (1997) R6333–R6336.
[9] X. He, L.S. Luo, Theory of the Boltzmann method: from the Boltzmann equation to the lattice Boltzmann equation, Phys. Rev. E 56 (1997) 6811–6817.
[10] D.O. Martinez, S. Chen, W. Matthaeus, Lattice Boltzmann magnetohydrodynamics, Phys. Rev. E 47 (1994) R2249–R2252.
[11] K. Gunstensen, D.H. Rothman, S. Zaleski, G. Zanetti, Lattice Boltzmann model of immiscible fluids, Phys. Rev. A 43 (1991) 4320–4327.
[12] D. Grunau, S. Chen, K. Eggart, A lattice Boltzmann model for multi-phase fluid flows, Phys. Fluids A 5 (1993) 2557–2562.

[13] C. Han-Taw, L. Jae-Yuh, Numerical analysis of hyperbolic heat conduction, Int. J. Heat Mass Transf. 36 (1993) 2891–2898.
[14] J.R. Ho, C.P. Kuo, W.S. Jiaung, C.J. Twu, Lattice Boltzmann scheme for hyperbolic heat conduction equation, Numer. Heat Transfer, Part B 41 (2002) 591–607.
[15] N. Gupta, G.R. Chaitanya, S.C. Mishra, Lattice Boltzmann method applied to variable thermal conductivity conduction and radiation problems, J. Thermophys. Heat Transfer 20 (2006) 895–902.
[16] J. Bernsdrof, G. Brenner, F. Durst, Numerical analysis of the pressure drop in porous media flow with lattice Boltzmann (BGK) automata, Comput. Phys. Commun. 129 (2000) 233–246.
[17] S. Chen, Z. Wang, X. Shan, G.D. Doolen, Lattice Boltzmann computational fluid dynamics in three dimensions, J. Stat. Phys. 68 (2000) 379–400.
[18] J. Hardy, Y. Pomeau, O. de Pazzis, Time evolution of a two-dimensional classical lattice system, Phys. Rev. Lett. 31 (1973) 276–279.
[19] U. Frisch, B. Hasslacher, Y. Pomeau, Lattice-gas automata for the Navier–Stokes equations, Phys. Rev. Lett. 56 (1986) 1505–1508.
[20] G. McNamara, G. Zanetti, Use of a Boltzmann equation to simulate lattice-gas automata, Phys. Rev. Lett. 61 (1988) 2332.
[21] F. Higuera, J. Jimenez, Boltzmann approach to lattice gas simulations, Europhys. Lett. 9 (1989) 663–668.
[22] P.L. Bhatnagar, E.P. Gross, M. Krook, A model for collision processes in gases. I. Small amplitude processes in charged and neutral one-component systems, Phys. Rev. 94 (1954) 511–525.
[23] J.M.V.A. Koelman, A simple lattice Boltzmann scheme for Navier–Stokes fluid flow, Europhys. Lett. 15 (1991) 603–607.
[24] S. Chen, H. Chen, Martinez, Matthaeus, Lattice Boltzmann model for simulation of magnetohydrodynamics, Phys. Rev. Lett. 67 (1991) 3776–3780.
[25] Y.H. Qian, D. d'Humieres, P. Lallamand, Lattice BGK models for Navier–Stokes equation, Europhys. Lett. 17 (1992) 479–484.
[26] H. Chen, S. Chen, W.H. Matthaeus, Recovery of the Navier–Stokes equation using a lattice-gas Boltzmann method, Phys. Rev. A 45 (1992) R5339–R5342.
[27] D.R. Noble, S. Chen, J.G. Georgiadis, R.O. Buckius, A consistent hydrodynamic boundary condition for the lattice Boltzmann method, Phys. Fluids 7 (1995) 203–209.
[28] T. Inamuro, M. Yoshino, F. Ogino, A non-slip boundary condition for lattice Boltzmann method, Phys. Fluids 7 (1995) 2928–2930.
[29] R.S. Maier, R.S. Bernard, D.W. Grunau, Boundary conditions for the lattice Boltzmann method, Phys. Fluids 8 (1996) 1788–1801.
[30] Q. Zou, X. He, On pressure and velocity boundary conditions for the lattice Boltzmann BGK model, Phys. Fluids 9 (1997) 1591–1598.
[31] O. Filippova, D. Hanel, Grid refinement for lattice-BGK models, J. Comput. Phys. 147 (1998) 219–228.
[32] R. Mei, L.S. Luo, W. Shyy, An accurate curved boundary treatment in the lattice Boltzmann method, J. Comput. Phys. 155 (1999) 307–330.
[33] M. Bouzidi, M. Firdaouss, P. Lallamand, Momentum transfer of a lattice Boltzmann fluid with boundaries, Phys. Fluids 13 (2001) 3452–3459.
[34] D. Yu, R. Mei, W. Shyy, A Unified Boundary Treatment in Lattice Boltzmann Method, American Institute of Aeronautics and Astronautics, New York, 2003 (2003-0953).
[35] D.A. Wolf-Gladrow, Lattice-Gas Cellular Automata and Lattice Boltzmann Models: An Introduction, Springer-Verlag, Berlin-Heidelberg, 2000.
[36] D. Yu, R. Mei, L.S. Luo, W. Shyy, Viscous flow computations with the method of lattice Boltzmann equation, Prog. Aerosp. Sci. 39 (2003) 329–367.
[37] D. A Perumal, G.V.S. Kumar, A.K. Dass, Application of Lattice Boltzmann method to fluid flows in microgeometries, CFD Lett. 2 (2010) 75–84.
[38] C. Cercignani, The Boltzmann Equation and Its Application, Springer, New York, 1988.
[39] D. A Perumal, A.K. Dass, Simulation of flow in two-sided lid-driven square cavities by the lattice Boltzmann method, Advances in Fluid Mechanics VII, vol. 45–54, Oxford University Press, United Kingdom, 2008.
[40] R. Mei, W. Shyy, D. Yu, L.S. Luo, Lattice Boltzmann method for 3-D Flows with curved boundary, J. Comput. Phys. 161 (2000) 680–699.
[41] P. Lallemand, L.S. Luo, Theory of the lattice Boltzmann method: dispersion, dissipation, isotropy, Galilean invariance, and stability, Phys. Rev. E 61 (2000) 6546–6562.
[42] D. d'Humieres, Generalized lattice Boltzmann equation in rarefied gas dynamics: theory and simulations, in: B.D. Shizgal, D.P. Weaver (Eds.), Prog. Astronaut. Aeronaut., vol. 159, AIAA, Washington, DC, 1992, pp. 450–458.
[43] J.-S. Wu, Y.-L. Shao, Simulation of lid-driven cavity flows by parallel lattice Boltzmann method using multi-relaxation-time scheme, Int. J. Numer. Methods Fluids 46 (2004) 921–937.
[44] C. Shu, Y. Peng, Y.T. Chew, Simulation of natural convection in a square cavity by Taylor series expansion and least squares based lattice Boltzmann method, Int. J. Mod. Phys. C 13 (2002) 1399–1414.
[45] W. Miller, Flow in the driven cavity calculated by the lattice Boltzmann method, Phys. Rev. E 51 (1995) 3659–3669.
[46] S. Hou, Q. Zou, S. Chen, G. Doolen, A.C. Cogley, Simulation of cavity Flow by the lattice Boltzmann method, J. Comput. Phys. 118 (1995) 329–347.
[47] B. Shi, N. He, N. Wang, Z. Guo, Lattice Boltzmann Simulations of Fluid Flows, vol. 24, Springer-Verlag, Berlin-Heidelberg, 2003, 322–332.
[48] S. De, K. Nagendra, K.N. Lakshmisha, Simulation of laminar flow in a three-dimensional lid-driven cavity by lattice Boltzmann method, Int. J. Numer. Methods Heat Fluid Flow 19 (2009) 790–815.
[49] D.V. Patil, K.N. Lakshmisha, Finite volume TVD formulation of lattice Boltzmann simulation on unstructured mesh, J. Comput. Phys. 228 (2009) 5262–5279.
[50] C. Shu, X.D. Niu, Y.T. Chew, Taylor series expansion and least squares-based lattice Boltzmann method: two-dimensional formulation and its applications, Phys. Rev. E 65 (2002) 036708-1–036708-13.
[51] D. A Perumal, A.K. Dass, Application of lattice Boltzmann method for incompressible viscous flows, Appl. Math. Model. 37 (2013) 4075–4092.
[52] M. Cheng, K.C. Hung, Vortex structure of steady flow in a rectangular cavity, Comput. Fluids 35 (2006) 1046–1062.
[53] D.V. Patil, K.N. Lakshmisha, B. Rogg, Lattice Boltzmann simulation of lid-driven flow in deep cavities, Comput. Fluids 35 (2006) 1116–1125.
[54] U. Ghia, K.N. Ghia, C.T. Shin, High-Re solutions for incompressible flow using the Navier–Stokes equations and a multigrid method, J. Comput. Phys. 48 (1983) 387–411.
[55] D. A Perumal, A.K. Dass, Simulation of incompressible flows in two-sided lid-driven square cavities. Part II – LBM, CFD Lett. 2 (2010) 25–38.
[56] D. A Perumal, A.K. Dass, Multiplicity of steady solutions in two-dimensional lid-driven cavity flows by lattice Boltzmann method, Comput. Math. Appl. 61 (2011) 3711–3721.
[57] G. McNamara, A.L. Garcia, B.J. Alder, Stabilization of thermal lattice Boltzmann models, J. Stat. Phys. 91 (1995) 395–408.

[58] J.G.M. Eggels, J.A. Somers, Numerical simulation of free convective flow using the lattice Boltzmann scheme, Int. J. Heat Fluid Flow 16 (1995) 357–364.
[59] X. He, S. Chen, G.D. Doolen, A novel thermal model for the lattice Boltzmann method in incompressible limit, J. Comput. Phys. 146 (1998) 282–300.
[60] X. Shan, Simulation of Rayleigh–Benard convection using a lattice Boltzmann method, Phys. Rev. E 55 (1997) 2780–2788.
[61] Y. Peng, C. Shu, Y.T. Chew, Simplified thermal lattice Boltzmann model for incompressible thermal flows, Phys. Rev. E 68 (2003) 026701–026708.
[62] J. Onishi, Y. Chen, H. Ohashi, Lattice Boltzmann simulation of natural convection in a square cavity, JSME Int. J. Ser. B 44 (2001) 53–62.
[63] F. Kuznik, J. Vareilles, G. Rusaouen, G. Krauss, A double-population lattice Boltzmann method with non-uniform mesh for the simulation of natural convection in a square cavity, Int. J. Heat Fluid Flow 28 (2007) 862–870.
[64] H.N. Dixit, V. Babu, Simulation of high Rayleigh number natural convection in a square cavity using the lattice Boltzmann method, Int. J. Heat Mass Transf. 49 (2006) 727–739.
[65] D. A Perumal, A.K. Dass, Lattice Boltzmann simulation of two- and three-dimensional incompressible thermal flows, Heat Transfer Eng. 35 (2014) 1320–1333.
[66] M. Yoshino, Y. Matsuda, C. Shao, Comparison of accuracy and efficiency between the lattice Boltzmann method and the finite difference Method in viscous/thermal fluid flows, Int. J. Comput. Fluid Dyn. 18 (2004) 333–345.
[67] M. Breuer, J. Bernsdorf, T. Zeiser, F. Durst, Accurate computations of the laminar flow past a square cylinder based on two different methods: lattice-Boltzmann and finite-volume, Int. J. Heat Fluid Flow 21 (2000) 186–196.
[68] S. Geller, M. Krafczyk, J. Tolke, S. Turek, J. Hron, Benchmark computations based on lattice-Boltzmann, finite element and finite volume methods for laminar flows, Comput. Fluids 35 (2006) 888–897.
[69] D.O. Martinez, W.H. Matthaeus, S. Chen, Comparison of spectral method and lattice Boltzmann simulations of two-dimensional hydrodynamics, Phys. Fluids 6 (1994) 1285–1298.
[70] X. He, G.D. Doolen, T. Clark, Comparison of the lattice Boltzmann method and the artificial compressibility method for Navier–Stokes equations, J. Comput. Phys. 179 (2002) 439–451.
[71] X. He, G. Doolen, Lattice Boltzmann method on curvilinear coordinates system: flow around a circular cylinder, J. Comput. Phys. 134 (1997) 306–315.
[72] D. A Perumal, G.V.S. Kumar, A.K. Dass, Lattice Boltzmann simulation of flow over a circular cylinder at moderate Reynolds numbers, Therm. Sci. 18 (2014) 1235–1246.
[73] S.U. Islam, C.Y. Zhou, Numerical simulation of flow around a row of cylinders using the lattice Boltzmann method, Inf. Technol. J. 4 (2009) 513–520.
[74] D.A. Perumal, G.V.S. Kumar, A.K. Dass, Numerical simulation of flow over a square cylinder using Lattice Boltzmann method, ISRN Math. Phys. 2012 (2012) 1–16.
[75] D.A. Perumal, G.V.S. Kumar, A.K. Dass, Lattice Boltzmann simulation of viscous flow past elliptic cylinder, CFD Lett. 4 (2012) 127–139.
[76] J. Tolke, M. Krafczyk, E. Rank, A multigrid-solver for the discrete Boltzmann equation, J. Stat. Phys. 117 (2002) 573–591.
[77] D.J. Mavriplis, Multigrid solution of the steady-state lattice Boltzmann equation, Comput. Fluids 35 (2006) 793–804.
[78] X. He, L.S. Luo, M. Dembo, Some progress in lattice Boltzmann method. Part I. Non-uniform mesh grids, J. Comput. Phys. 129 (1996) 357–363.
[79] F. Kuznik, J. Vareilles, G. Rusaouen, G. Krauss, A double-population lattice Boltzmann method with non-uniform mesh for the simulation of natural convection in a square cavity, Int. J. Heat Fluid Flow 28 (2007) 862–870.
[80] S.C. Mishra, B. Mondal, T. Kush, B.S.R. Krishna, Solving transient heat conduction problems on uniform and non-uniform lattices using the lattice Boltzmann method, Int. Commun. Heat Mass Transfer 36 (2009) 322–328.
[81] T. Inamuro, A lattice kinetic scheme for incompressible viscous flows with heat transfer, Philos. Trans. R. Soc. London A 360 (2002) 477–484.
[82] D. A Perumal, A.K. Dass, Computation of Lattice kinetic scheme for double-sided parallel and antiparallel wall motion, Appl. Mech. Mater. 592-594 (2014) 1967–1971.
[83] Y. Peng, C. Shu, Y.T. Chew, Lattice kinetic schemes for incompressible viscous thermal flows on arbitrary meshes, Phys. Rev. E 69 (2004) 016731–016738.
[84] M. Mendoza, J.-D. Debus, S. Succi, H.J. Herrmann, Lattice kinetic scheme for generalized coordinates and curved spaces, Int. J. Mod. Phys. C 25 (2014) 1441001–1441010.
[85] F.J. Alexander, H. Chen, S. Chen, G.D. Doolen, Lattice Boltzmann model for compressible fluids, Phys. Rev. A 46 (1992) 1967–1970.
[86] Y. Chen, H. Ohashi, M. Akiyama, Thermal lattice Bhatnagar–Gross–Krook model without nonlinear derivations in macrodynamic equations, Phys. Rev. E 50 (1994) 2776–2783.
[87] G. Yan, Y. Chen, S. Hu, Simple lattice Boltzmann model for simulating flows with shock wave, Phys. Rev. E 59 (1999) 454–459.
[88] H. Yu, K. Zhao, Lattice Boltzmann method for compressible flows with high Mach numbers, Phys. Rev. E 61 (2000) 3867–3870.
[89] B. Palmer, D. Rector, Lattice Boltzmann algorithm for simulating thermal flow in compressible fluids, J. Comput. Phys. 161 (2000) 1–20.
[90] T. Kataoka, M. Tsutahara, Lattice Boltzmann model for the compressible Navier–Stokes equations with flexible specific-heat ratio, Phys. Rev. E 69 (2004) 0357011–0357014.
[91] C. Sun, Lattice-Boltzmann models for high speed flows, Phys. Rev. E 58 (1998) 7283–7287.
[92] C. Sun, A. Hsu, Multi-level lattice Boltzmann model on square lattice for compressible flows, Comput. Fluids 33 (2004) 1363–1385.
[93] B. He, Y. Chen, W. Feng, Q. Li, A. Song, Y. Wang, M. Zhang, W. Zhang, Compressible lattice Boltzmann method and applications, Int. J. Numer. Anal. Model. 9 (2012) 410–418.
[94] K. Li, C. Zhong, A lattice Boltzmann model for simulation of compressible flows, Int. J. Numer. Meth. Fluids 77 (2015) 334–357.
[95] I. Ginzburg I, K. Steiner, Lattice Boltzmann model for free-surface flow and its application to filling process in casting, J. Comput. Phys. 185 (2003) 61–99.
[96] C. Körner, M. Thies, T. Hofmann, N. Thurey, U. Rude, Lattice Boltzmann model for free surface flow for modeling foaming, J. Stat. Phys. 121 (2005) 179–196.
[97] Y. Yu, L. Chen, J. Lu, G. Hou, A coupled lattice Boltzmann and particle level set method for free surface flows, ScienceAsia 40 (2014) 238–247.
[98] C. Janssen, M. Krafczyk, A lattice Boltzmann approach for free-surface-flow simulations on nonuniform block-structured grids, Comput. Math. Appl. 59 (2010) 2215–2235.
[99] K.E. Wardle, T. Lee, Finite element lattice Boltzmann simulations of free surface flow in a concentric cylinder, Comput. Math. Appl. 65 (2013) 230–238.
[100] A. Leonardi, F.K. Wittel, M. Mendoza, H.J. Herrmann, Coupled DEM-LBM method for the free-surface simulation of heterogeneous suspensions, Comput. Particle Mech. 1 (2014) 3–13.
[101] M. Gad-el-Hak, The fluid mechanics of microdevices-the freeman scholar lecture, J. Fluids Eng. 121 (1999) 6–33.

[102] X.D. Niu, C. Shu, Y.T. Chew, Lattice Boltzmann BGK model for simulation of micro flows, Euro Phys. Lett. 67 (2004) 600–606.
[103] D. Raabe, Overview of the lattice Boltzmann method for nano- and microscale fluid dynamics in materials science and engineering, Modell. Simul. Mater. Sci. Eng. 12 (2004) 13–46.
[104] D. A Perumal, V. Krishna, G. Sarvesh, A.K. Dass, Numerical simulation of gaseous microflows by lattice Boltzmann method, Int. J. Recent Trends Eng. 1 (2009) 15–20.
[105] C.Y. Lim, C. Shu, X.D. Niu, Y.T. Chew, Application of the lattice Boltzmann method to simulate microchannel flows, Phys. Fluids 14 (2002) 2209–2308.
[106] X. Nie, G.D. Doolen, S. Chen, Lattice-Boltzmann simulations of fluid flows in MEMS, J. Stat. Phys. 107 (2002) 279–289.
[107] S. Ansumali, I.V. Karlin, C.E. Frouzakis, K.B. Boulouchos, Entropic lattice Boltzmann method for microflows, Phys. A 359 (2006) 289–305.
[108] F. Verhaeghe, L.S. Luo, B. Blanpain, Lattice Boltzmann modeling of microchannel flow in slip flow regime, J. Comput. Phys. 228 (2009) 147–157.
[109] S. Alapati, S. Kang, Y.K. Suh, Parallel computation of two-phase flow in a microchannel using the lattice Boltzmann method, J. Mech. Sci. Technol. 23 (2009) 2492–2501.
[110] K. Suga, Lattice Boltzmann methods for complex micro-flows: applicability and limitations for practical applications, Fluid Dyn. Res. 45 (2013) 034501.